Volume 48 http://acousticalsociety.org/

22nd International Symposium on Nonlinear Acoustics
Oxford, UK
4-8 July 2022

Engineering Acoustics: Session 11 NDE

Effects of narrow bandwidth signal for coherent nonlinear array imaging

Zubeir Muhammad Ebrahim Saib, Bruce W. Drinkwater and Anthony J. Croxford
Department of Mechanical Engineering, University of Bristol, Bristol, Avon, BS8 1TR, UNITED KINGDOM; z.ebrahimsaib@bristol.ac.uk; me15901@my.bristol.ac.uk; B.Drinkwater@bristol.ac.uk; A.J.Croxford@bristol.ac.uk

Nonlinear ultrasound has shown its sensitivity to early formation of defects such as micro-cracking and material aging. When an ultrasonic wave propagates in a nonlinear material, there is transfer of energy from the fundamental frequency to its harmonics. This energy loss can be used for spatial mapping of nonlinearity within sample using arrays. In this study, we investigate the effects of the input signal and instrument over the nonlinear measurement. To this end, a two dimensional finite difference numerical simulation has been created to model nonlinear elastic wave propagation. It was used to investigate, from a sensitivity to damage perspective, the difference between focused transmission and sequential firing of elements while focusing is performed in post processing. The model allows energy from the coherent scattered field within the material to be monitored, which is not possible in real experiments. The result shows the influence of the bandwidth of the input signal on the nonlinear measurement. This was experimentally investigated on a sample with a surface breaking crack acting as a high local nonlinearity region. Nonlinear images showed an increase in sensitivity with narrowband signals, at the expense of resolution.

Published by the Acoustical Society of America

 https://doi.org/10.1121/2.0001667

1. INTRODUCTION

Nonlinear ultrasonic techniques (NUTs) have shown their sensitivity to the early formation of damage[1–3] as the creation of micro-defects is associated with a localised increase in material nonlinearity. The interaction of these defects with an ultrasonic signal shifts energy to harmonic frequencies. Higher harmonics are seen for material nonlinearity, and additionally subharmonic frequencies for closed cracks.[4,5] As such, detection of nonlinearity can be achieved either by probing the harmonic frequencies, or looking at the energy loss from the fundamental frequency.

With the recent advent of arrays, there has been an increased interest in nonlinear array imaging. Subharmonic imaging showed that the closed portion of a crack tip can be detected with NUT.[4] Due to the low frequency at reception for subharmonic imaging, the spatial resolution of the image is typically poor. To improve the resolution, reception was done at the input signal frequency, and the fundamental wave amplitude difference (FAD) technique was introduced.[6] This uses the scaling subtraction method (SSM)[7] whereby the assumption made is that there is no nonlinear response at low amplitude. The even-odd firing scheme[5,8] has also been explored, which was later proven to be superior to SSM.[5] Building on this, a scheme using sequential firing of elements (based on the full matrix capture[9]), which was initially used for diffuse field imaging,[10] was applied to the coherent field response.[11] In all of the above mentioned cases, they are two linearly equivalent transmission modes, and hence the residual obtained from the subtraction of the two images is used as a way to characterise nonlinearity.

In this work, we assess the sensitivity of the parallel-sequential firing scheme for coherent field nonlinear imaging. A numerical model based on the finite difference method is used to solve the nonlinear wave equation to better understand the difference in energy at the focal spot between the two transmission modes. We stress the importance of the model as it tracks movement of energy between frequency components, which is essential to understand the physical phenomena that govern the experiments to enable better measurement techniques in order to increase sensitivity.

2. NUMERICAL MODEL

This section introduces the numerical model used in this study to simulate parallel-sequential firing to better understand contribution from material nonlinearity.

A. MATHEMATICAL FORMULATION AND IMPLEMENTATION

The nonlinear wave equations used in this study are derived and presented elsewhere.[12] We quote the main results that are implemented in the simulation. Using the Einstein summation convention, the geometrical nonlinearity is considered in the strain tensor:

$$\varepsilon_{ij} = \frac{1}{2}\left(\frac{\partial u_i}{\partial x_j} + \frac{\partial u_j}{\partial x_i} + \frac{\partial u_k}{\partial x_i}\frac{\partial u_k}{\partial x_j}\right), \tag{1}$$

where i and j are coordinate directions and u is the particle displacement. The components of the stress tensor can be obtained from

$$\sigma_{ij} = \frac{\partial \mathcal{E}(I_1, I_2, I_3, E, \nu, \mathcal{A}, \mathcal{B}, \mathcal{C})}{\partial(\partial u_i/\partial x_j)}, \tag{2}$$

where $\mathcal{E}$ is the strain energy density, which is a function of the invariants of the strain tensor (I_1, I_2 and I_3), E and ν are the Young's modulus and Poisson's ratio respectively, and the three third order elastic constants $\mathcal{A}$, $\mathcal{B}$ and $\mathcal{C}$. Finally, the nonlinear wave equation for a material of uniform density ρ can be derived using

$$\rho\frac{\partial^2 u_i}{\partial t^2} = \frac{\partial \sigma ij}{\partial x_j}. \tag{3}$$

The above equations for nonlinear wave propagation are discretised and solved using the finite difference method. A high order centred scheme is used for spatial gradient calculations. A convergence study previously carried out showed that the distance step (Δx_1 and Δx_3) should be at least $\lambda_s/18$, where λ_s is the smallest wavelength being modelled. This is consistent with previous work.[13] Here, we chose $\Delta x_1 = \Delta x_3 = \lambda_s/20$ for better accuracy, where our smallest wavelength of interest is the second harmonic of the input signal.

A stress-type boundary condition is applied for the input, while free surfaces are used on the remaining nodes on the boundary. The implementation of the excitation of the array is performed element-wise, by exciting a series of nodes found within the spatial location of each element. A smoothing function is applied to remove discontinuity in displacement at the element edges. Nodes within each element have the same delay when phased-array type focusing is required.

B. PREDICTION FOR PARALLEL-SEQUENTIAL FIRING

We use the above model to consider the parallel-sequential firing scheme used for nonlinear array imaging in a uniformly nonlinear material. These are two linearly equivalent modes of transmission, i.e. applying delays to the sequentially-captured data in post-processing should, if linear superposition holds, result in the same amplitude at the focal spot as seen in the parallel transmission mode. However, this is not the case due to nonlinearity, and was exploited previously.[10,11] In this section, we simulate this effect to demonstrate the contribution coming from material nonlinearity. As a virtual experiment, a 64 element array of centre frequency (f_0) of 5 MHz is focused at a depth of 15 mm in an aluminium sample with material properties given in Table 1. Each element is modelled by exciting a series of nodes located within the region of the element. The element pitch and spacing are 0.6 and 0.1 mm respectively. These are based on the design of the array being used in the experiment (Imasonic, France, model 12157 1001).

In this study, we monitor the vertical component of displacement as this is typically measured by the array in the real experimental setup. It is straightforward to obtain the data for the parallel transmission case by phasing the outputs of the elements to achieve the desired focus. As for the sequential case, it is possible to use the same numerical model (code-wise) by firing only one element at a time with the same delay applied as in the parallel case. However, this is computationally expensive. Due to uniform nonlinearity, an alternative of firing a single transducer can be used. In this model, the signal of all nodes at a depth of 15 mm parallel to the surface is recorded (see Fig. 1(a)). With the appropriate radial vector from the element to the focal point, the node from the single transducer model required for the sequentially captured data can be extracted (left panel in Fig. 1(b)). The delays applied in the parallel transmission simulation are then used to obtain the delayed signal required for each other element (refer to right panel of Fig. 1(b)).

Summing over the signals from each element after applying the delay gives the signal from the sequential case at the focal point. A time domain comparison between the parallel ($A_p(t)$) and sequential ($A_s(t)$)

Table 1: Linear and nonlinear material constants of Aluminium used throughout this paper.

Parameter	Symbol	Value	Unit
Density	ρ	2700	kg/m^3
Young's modulus	E	69	GPa
Poisson ratio	ν	0.33	-
Third order elastic constants	$\mathcal{A}$	-344	GPa
	$\mathcal{B}$	-124	GPa
	$\mathcal{C}$	-19.5	GPa

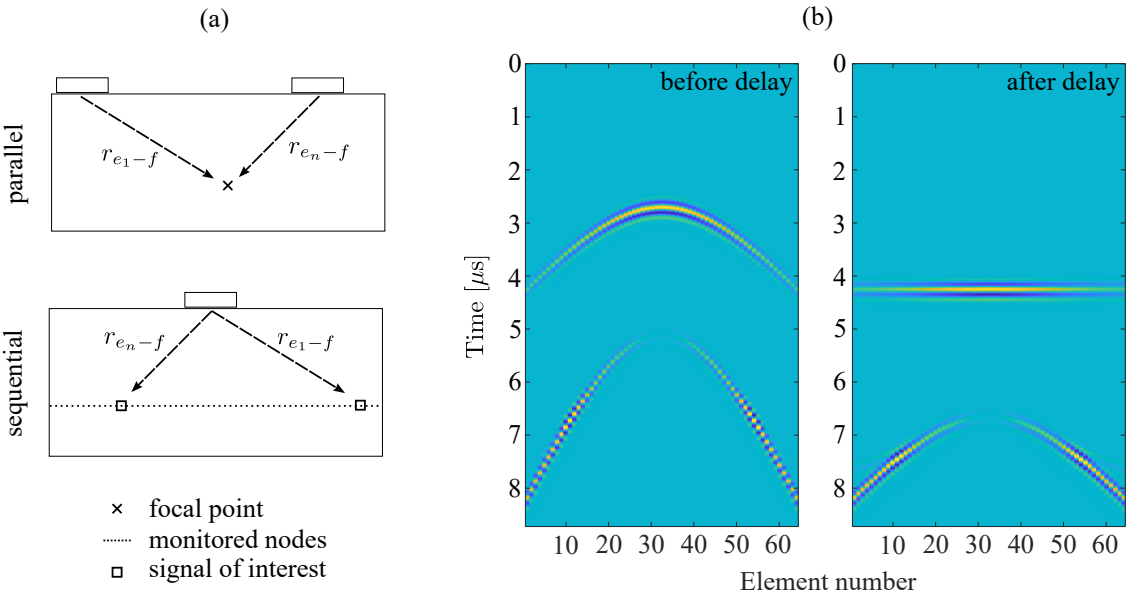

Figure 1: (a) Illustration of how a single transducer model is used to obtain the sequentially captured signal and (b) application of delays to obtain the signal at the focal point.

transmission case for a 3 cycle Hanning windowed function at 5 MHz with input amplitude 1 MPa is shown in top panel of Fig. 2(a). The amplitude of the nonlinear metric measured in the simulation is

$$A_m(t) = A_s(t) - A_p(t) \tag{4}$$

and is shown in the bottom panel of Fig. 2(a).

A better comparison of the two transmission cases can be studied in the frequency domain. Here, a half bandwidth of $\frac{1}{6}f_0$ is used to limit any internal movement of energy.[11] The fast fourier transform (FFT) of each signal is taken. The amplitude ratio

$$\delta_A(\omega) = \frac{A_s(\omega)}{A_p(\omega)} \tag{5}$$

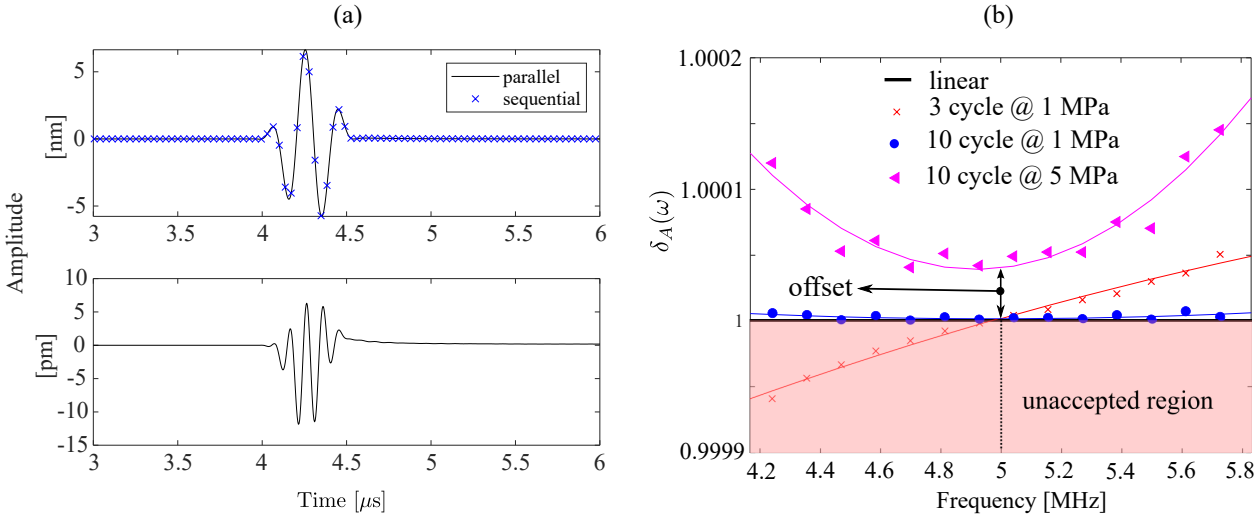

Figure 2: Nonlinear signal at the focal point in (a) time and (b) frequency domain.

gives an indication of the difference between the two transmission cases. Due to material nonlinearity, we expect $\delta_A > 1 \; \forall \; \frac{5}{6} f_0 \leq f \leq \frac{7}{6} f_0$ since $A_p(\omega)$ loses more energy to harmonic frequencies (because of high focal amplitude) compared to $A_s(\omega)$.

Figure 2(b) shows that part of the bandwidth is less than 1 for a 3 cycle input. This is explained as internal movement of energy between the harmonic frequencies and the main lobe at f_0 due to the signal being broadband. Increasing the number of cycles to 10 makes the signal more narrowband and pushes all the values of $\delta_A(\omega)$ above 1. The implication of material nonlinearity can be seen when the input amplitude is increased to 5 MPa to make the nonlinearity more detectable, as shown in Fig. 2(b). A parabolic trend with frequency is noted, where an offset at the centre frequency is introduced due to material nonlinearity. This is the effect of the parallel transmission losing more energy at the focal spot relative to the sequential scheme due to higher amplitude. However, contributions from material nonlinearity are low as seen from δ_A being approximately equal to 1. Neglecting attenuation, this would be the δ_A one would expect from an undamaged backwall reflection during a pulse-echo measurement.

3. EXPERIMENTAL RESULTS

This section focuses on the experimental measurements carried out for this study. A sample with a surface breaking crack is used to assess the contribution of experimental nonlinearity, and how effective the suppression used by Cheng et al.[11] is. The implication of having a narrowband signal is also studied.

A. NONLINEAR CALIBRATION

An array of 64 elements operating at 5 MHz is used for transmission and reception. A 3 cycle input at peak voltage amplitude of 50 V is used initially. The imaging region is selected to be around the backwall, and focusing is performed at each imaging pixel. The full matrix capture method is used to obtain sequentially-captured data. The pixel-wise delay applied for the parallel transmission is used in post-processing to adjust the sequential captured signals for appropriate imaging. The raw result obtained from the experiment is shown in Fig. 3. The nonlinear image is obtained by subtracting the parallel image intensity from the sequential one. We note that there is not enough suppression of the linear backwall geometric feature in the nonlinear image (as seen in Fig. 3(c)).

To assess the effect of instrumental nonlinearity, 15 pixels along the backwall (considered undamaged) on either end were used to calculate the required correction introduced by Cheng et al.[11] The pixels are shown in white boxes in Fig. 3(a) and (b). The value of δ_A for those pixels are calculated by taking the

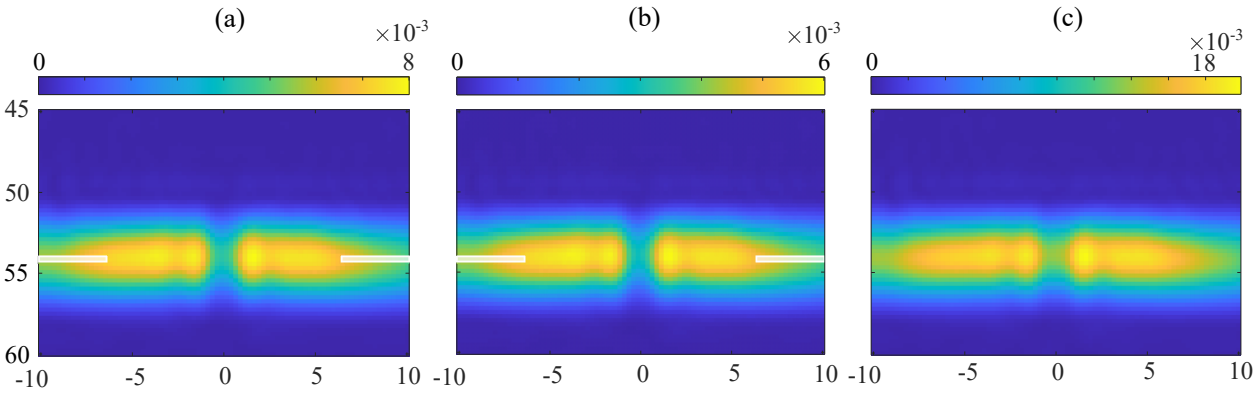

Figure 3: (a) Sequential, (b) parallel and (c) nonlinear image obtained without correction. Pixels used for applying correction are shown in white boxes.

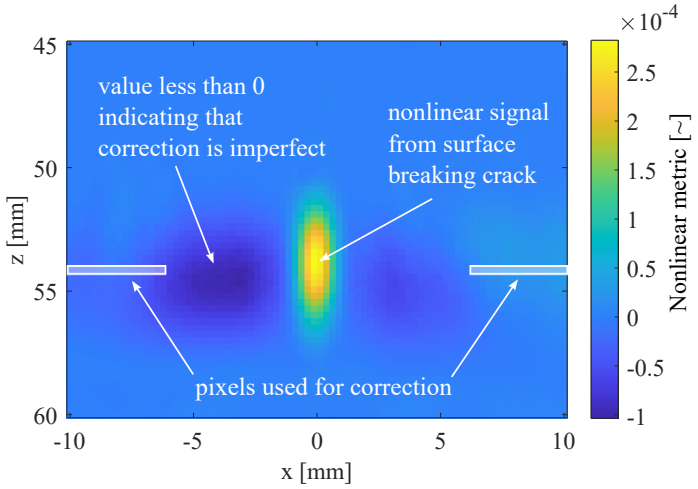

Figure 4: Corrected nonlinear image. Values below 0 ***shows imperfection in correction applied.***

ratio according to Eq. (5). Assuming the crack tip nonlinearity is larger than the surrounding material nonlinearity, it is reasonable to assume that $\delta_A = 1$ for the pixels within the white box in Fig. 3(a) and (b). This also makes the assumption implicitly that the backwall is behaving as a linear scatterer. Hence, all nonlinear measurements being carried out in this study are assumed to be relative to those pixels. Similar correction to the phase difference between the parallel and sequential captured data can be made, but here we are only interested in the amplitude image. Note that this scaling in the imaging metric attempts at suppressing classical materian and instrumental nonlinearity.[11]

Previous work[11] showed the nonlinear image as an absolute value. Here, we calculate only the subtraction $A_s - A_p$ as it is essential to ensure that $A_s \geq A_p$ after applying the correction within the imaging region. By not taking the absolute of the image, imperfection from the behaviour of the instrumental setup manifests. This can be seen as the low amplitude region ($\delta_A < 0$) on either sides (mostly on the left) of the nonlinear point spread function (NPSF) in Fig. 4. It suggests that the array is unable to produce symmetrical signals when focus on either sides of its symmetry line. One possible implication is that a correction that is spatially-dependent on the imaging location is required as a different value of δ_A should be used to ensure $\delta_A \geq 0$ within the imaging region. However, obtaining this spatially-dependent correction is impossible unless the behaviour of the array is properly understood or controlled.

B. IMPLICATION OF NARROWBAND SIGNALS

With the importance of having narrowband signals shown from the simulation to prevent internal movement of energy within the main excitation bandwidth, this is analysed experimentally. Here, the number of cycles is increased and the amplitude of the peak within the nonlinear image is measured. The experiment is repeated 5 times for each cycle number without changing the coupling condition. Further to this, the specimen is cleaned, and a new set of coupling is applied and the experiment is repeated. The peak voltage is kept the same for all experiments, whilst the reception gain is changed for better detectability due to different coupling transfer functions.

The maximum of the NPSF in Fig. 4 as the number of input cycles is varied is shown in Fig. 5(a). Independent of the coupling conditions, a clear increasing trend in the peak of the nonlinear metric is seen with increasing number of cycles. The small size of error bars shows that the array and controller can reliably produce the same waveform.

However, increasing the number of cycles effectively increases the input energy into the material at the fundamental frequency. As normalisation, the maximum nonlinear metric in Fig. 5(a) is divided by the

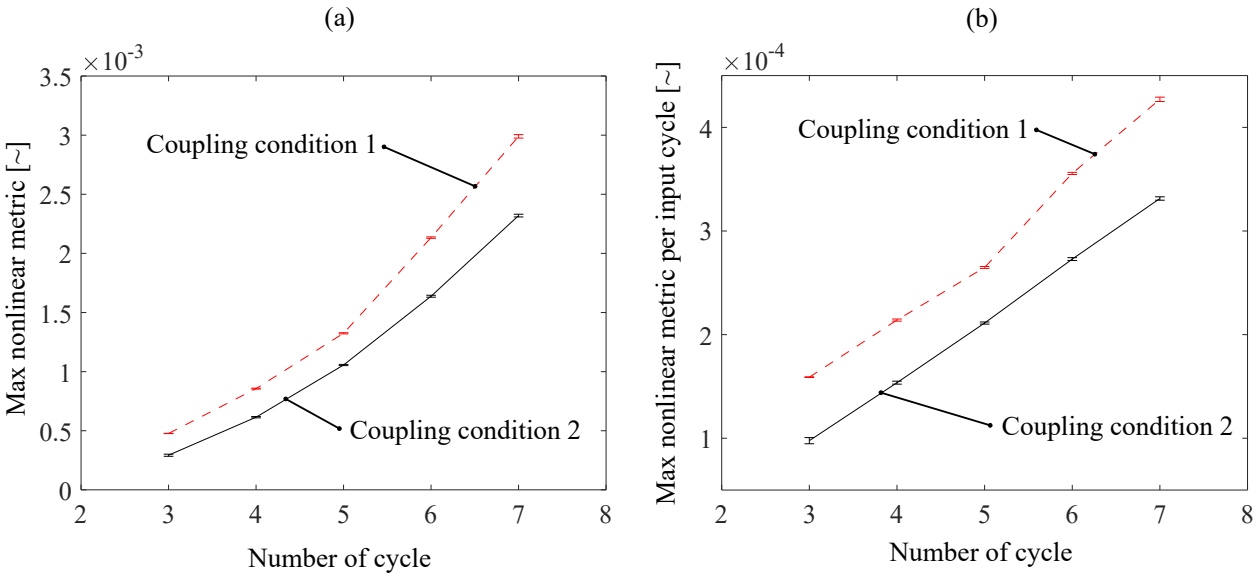

Figure 5: Dependence of the (a) nonlinear metric and (b) normalised nonlinear metric with the number of cycles used as input. Note that error bars are shown on both results. Different coupling conditions are shown with different line types.

input cycle used and is shown in Fig. 5(b). For both coupling conditions, a clear linear increase with input number of cycles is noticed, indicating that the imaging system becomes more sensitive to damage as it has a larger dynamic range for measurements. Hence, with an attempt at reducing internal movement of energy by using narrowband signals, an increase in nonlinear measurement sensitivity is seen.

It should also be noted that increasing the number of cycles decreases the spatial resolution of the image. Here, we assess how this affects the nonlinear image, which is now being constructed from the individually-degraded linear images. For each set of measurements, the size of the local nonlinearity is measured using the 6 dB drop rule. Its variation as the number of cycles is altered is shown in Fig. 6. Interestingly, there is less variation in the spread of the nonlinearity when the input cycle is 4, as seen by the small errorbars for both coupling conditions. The change in the size of the nonlinearity remains relatively

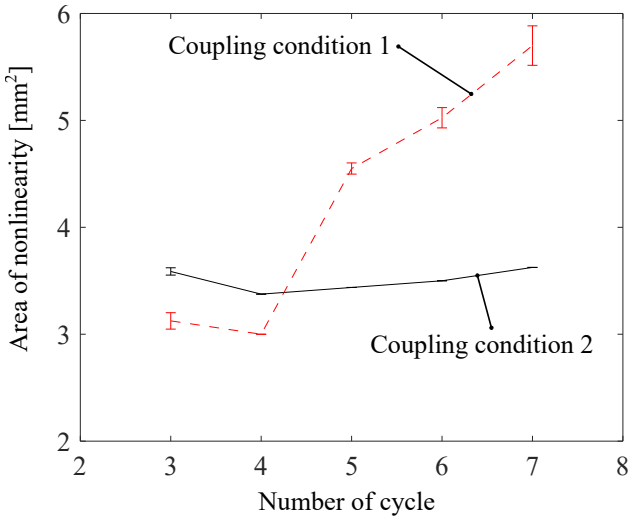

Figure 6: Measured area of local nonlinearity above a 6 dB threshold as number of cycle is varied.

constant when the cycle number is increased from 3 to 4. This is because the measurement is limited by the bandwidth of the transducer for small number of cycles (i.e. changing the number of cycle in the input signal for the transducer does not change the resulting output being transmitted into the material due to the transfer function of the transducer). For cycle number higher than 4, an increase in the size of the measured nonlinearity is seen, irrespective of the coupling condition. However, the range of change in the spread is different for each coupling condition. This could possibly be due to uneven coupling layer in between the array and the material surface and is difficult to control. It results in the transmission coefficient of some particular elements being higher, hence favouring a specific pixel which gets amplified with increasing number of cycles. However, both coupling conditions show an increase in the NPSF with increasing number of cycles, indicating degrading resolution similar to linear imaging algorithm.

4. CONCLUSION

A numerical model, based on the finite difference method, was built to solve the nonlinear wave equations. It was used to simulate the array behaviour of parallel-sequential coherent field subtraction technique to assess contribution from material nonlinearity, which was shown to be negligible. Experimental measurements were carried out using the parallel-sequential coherent field subtraction technique following the work of Cheng et al.[11] By only measuring the difference between the amplitude of the sequential and parallel firing, without taking the absolute and after applying appropriate compensation,[11] the imperfection of the behaviour of the instrument was revealed. This can be corrected through, either the better understanding of the instrument, or through the application of a pixel-wise correction factor. Finally, the importance of having narrower bandwidth was studied, which showed improved sensitivity to damage at the expense of resolution.

ACKNOWLEDGEMENTS

This work was supported by funding from Engineering and Physical Sciences Research Council (EPSRC) for the Centre of Doctoral Training in Future Innovation in Non destructive Evaluation (FIND) and the University of Bristol.

REFERENCES

[1] J. H. Cantrell and W. T. Yost, "Nonlinear ultrasonic characterization of fatigue microstructures", *Int. J. Fat.* **23**, 487-490 (2001).

[2] A. J. Croxford, P. D. Wilcox and P. B. Nagy, "Nonlinear ultrasonic characterization of fatigue microstructures", *J. Acoust. Soc. Am.* **126**, 117-122 (2009).

[3] G. Tang, M. Liu and L. J. Jacobs, "Detecting localized plastic strain by a scanning collinear wave mixing method", *J. Nond. Eval.* **33**, 196-204 (2014).

[4] Y. Ohara, T. Mihara, R. Sasaki, T. Ogata, S. Yamamoto, Y. Kishimoto and K. Yamanaka, "Imaging of closed cracks using nonlinear response of elastic waves at subharmonic frequency", *Appl. Phys. Lett.* **90**, 011902 (2007).

[5] Y. Ohara, H. Nakajima, S. Haupert, T. Tsuji and T. Mihara, "Nonlinear ultrasonic phased array with fixed-voltage fundamental wave amplitude difference for high-selectivity imaging of closed cracks", *J. Acoust. Soc. Am.* **146**, 266-277 (2019).

[6] M. Ikeuchi, K. Jinno, Y. Ohara and K. Yamanaka, "Improvement of closed crack selectivity in nonlinear ultrasonic imaging using fundamental wave amplitude difference", *Jpn. J. Appl. Phys.* **52**, 07HC08 (2013).

[7] M. Scalerandi, A. S. Gliozzi, C. L. E. Bruno, D. Masera and P. Bocca, "A scaling method to enhance detection of a nonlinear elastic response", *Appl. Phys. Lett.* **92**, 101912 (2008).

[8] S. Haupert, G. Renaud and A. Schumm, "Ultrasonic nonlinear imaging of scatterers buried in a medium", *NDT & E Int.* **87**, 1-6 (2017).

[9] C. Holmes, B. W. Drinkwater and P. D. Wilcox, "Post-processing of the full matrix of ultrasonic transmit-receive array data for non-destructive evaluation", *NDT & E Int.* **8**, 701-711 (2005).

[10] J. N. Potter, A. J. Croxford and P. D. Wilcox, "Nonlinear ultrasonic phased array imaging", *Phys. Rev. Lett.* **113**, 144301 (2014).

[11] J. Cheng, J. N Potter and B. W. Drinkwater, "The parallel-sequential field subtraction technique for coherent nonlinear ultrasonic imaging", *Smart Mater. Struct.* **27**, 065002 (2018).

[12] K. R. McCall, "Theoretical study of nonlinear elastic wave propagation", *J. Geo. Res.* **99**, 2591-2600 (1994).

[13] R. S. Mini, P. Ravindran, C. V. Krishnamurthy and K. Balasubramaniam, "Experimental and numerical investigation of second harmonic generation by creep induced micro-voids", *Exp. Mech.* **60**, 1017-1032 (2020).